In Situ Detection of the Adsorbed Fe(II) Intermediate and the Mechanism of Magnetite Electrodeposition by Scanning Electrochemical Microscopy

Mohsin A. Bhat,[⊥,†] Nikoloz Nioradze,[‡] Jiyeon Kim,[§] Shigeru Amemiya,[¶] and Allen J. Bard*[,⊥]

[⊥]Center for Electrochemistry, Department of Chemistry, The University of Texas at Austin, Austin, Texas 78712, United States
[†]Department of Chemistry, University of Kashmir, Srinagar 190006, Jammu and Kashmir, India
[‡]The R. Agladze Institute of Inorganic Chemistry and Electrochemistry, Ivane Javakhishvili Tbilisi State University, Tbilisi 0179, Georgia
[§]Department of Chemistry, The University of Rhode Island, Kingston, Rhode Island 02881, United States
[¶]Department of Chemistry, University of Pittsburgh, Pittsburgh, Pennsylvania 15260, United States

S *Supporting Information*

ABSTRACT: Electrodeposition is an important approach that can produce functional compound materials by assembling multiple species at the electrode surface. However, a fundamental understanding of the electrodeposition mechanism has been limited by its complexity and is often gained only through ex situ studies of deposited materials. Here we report on the application of scanning electrochemical microscopy (SECM) to enable the in situ, real-time, and quantitative study of electrodeposition and electrodissolution. Specifically, we electrodeposit magnetite (Fe_3O_4) from an alkaline solution of $Fe(III)$−triethanolamine as a robust route that can prepare this magnetic and electrocatalytic compound on various conductive substrates. The powerful combination of SECM with cyclic voltammetry (CV) at a gold substrate reveals that the electrodeposition of magnetite requires the preceding adsorption of $Fe(II)$−triethanolamine on the substrate surface and, subsequently, is mediated through the highly complicated $EC_{ads}C_{mag}$ mechanism, where both chemical steps occur at the substrate surface rather than in the homogeneous solution. SECM-based CV is obtained under high mass-transport conditions and analyzed by the finite element method to kinetically resolve all steps of the $EC_{ads}C_{mag}$ mechanism and quantitatively determine relevant reaction parameters. By contrast, the adsorbed $Fe(II)$ intermediate is unresolvable from co-deposited magnetite in situ by other electrochemical techniques and is undetectable ex situ because of the facile air oxidation of the $Fe(II)$ intermediate. Significantly, SECM-based CV will be useful for the in situ characterization of various electrodeposited compounds to complement their ex situ characterization.
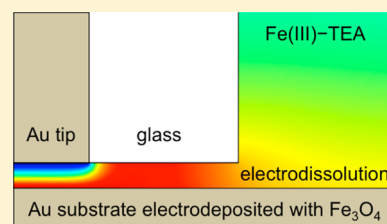
INTRODUCTION

Electrodeposition has been of recent interest owing to its capability to produce not only simple elemental materials but also compound materials with advanced functions.[1] Electrodeposited films of multielement compounds such as mixed metal oxides,[2] multinary semiconductors,[3] and perovskite absorbers[4] are attractive for a wide range of applications including electrocatalysis,[5] photocatalysis,[6] and solid-state semiconductor devices.[7] It, however, is highly challenging to understand the mechanism of electrodeposition of compound materials, which is complicated by the coupling of chemical reactions with electron-transfer (ET) reactions at the substrate electrode surface.[1] Moreover, the electrodeposition of compound materials involves chemical reactions of multiple species that are transported from the solution to the surface or adsorbed on the surface, often as a prelude to nucleation and growth of a bulk solid phase. Accordingly, the structure, morphology, and composition of electrodeposited compounds depend on the dynamic availability of species near and on the substrate surface in addition to the substrate potential.
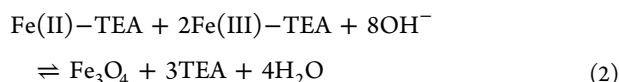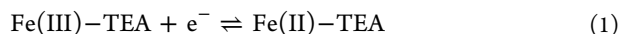
Nevertheless, surface intermediate species are not electrochemically resolvable from the final product either in situ or ex situ.[7,8] The spectroscopic and microscopic characterization of an electrodeposited film is usually performed ex situ[7,8] to obtain no real-time information about electrodeposition kinetics and manifest the alternation of film composition, for example, through air oxidation.[9]

Herein, we report on new mechanistic insights into the electrodeposition of magnetite (Fe_3O_4)[10] as a multifunctional compound that is attractive for magnetic memory devices,[11] electrocatalytic oxygen reduction,[12] and lithium-ion batteries.[13] Specifically, we investigate the versatile route that has been established by Switzer and co-workers[9] to electrodeposit magnetite on various conductive substrates, for example, gold,[9,11b,14] copper,[13,15] nickel,[16] indium tin oxide,[12c] stainless steel,[9,11c,14] carbon steel,[17] and highly oriented pyrolytic graphite,[9] from an alkaline solution of $Fe(III)$−triethanolamine
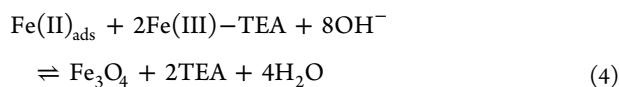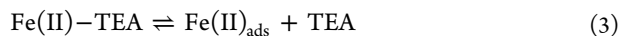
(TEA), where in all complexes, TEA represents two TEA ligands. Recently, the Fe(III)−TEA/Fe(II)−TEA couple was also used for alkaline redox flow batteries,[18] thereby requiring a better mechanistic understanding of when and how magnetite electrodeposits. More fundamentally, previous studies[9,14] presumed that magnetite is electrodeposited through the EC mechanism, where the reduction of Fe(III)−TEA at the substrate surface is followed by the one-step deposition of magnetite, that is,

$$\text{Fe(III)}-\text{TEA} + e^- \rightleftharpoons \text{Fe(II)}-\text{TEA} \qquad (1)$$

$$\text{Fe(II)}-\text{TEA} + 2\text{Fe(III)}-\text{TEA} + 8\text{OH}^-$$
$$\rightleftharpoons \text{Fe}_3\text{O}_4 + 3\text{TEA} + 4\text{H}_2\text{O} \qquad (2)$$

However, an ex situ study revealed that the electrodeposited films were nonstoichiometric magnetite containing an excess amount of Fe(III).[9] Moreover, ferrihydrite (hydrated Fe_2O_3) was obtained at unexpectedly negative potentials, which was attributed to the electrodeposition and air oxidation of green rust (a mixed Fe(II)−Fe(III) hydroxide).[9]

In this work, we apply scanning electrochemical microscopy[19] (SECM) to reveal that the electrodeposition of magnetite from an alkaline Fe(III)−TEA solution requires the preceding formation of the Fe(II) intermediate adsorbed on the substrate surface. We demonstrate quantitatively that Fe(II)−TEA is generated at (eq 1) and adsorbed on the substrate surface to form the intermediate, Fe(II)$_{ads}$, which reacts with Fe(III)−TEA transported from the solution to deposit magnetite, that is,

$$\text{Fe(II)}-\text{TEA} \rightleftharpoons \text{Fe(II)}_{ads} + \text{TEA} \qquad (3)$$

$$\text{Fe(II)}_{ads} + 2\text{Fe(III)}-\text{TEA} + 8\text{OH}^-$$
$$\rightleftharpoons \text{Fe}_3\text{O}_4 + 2\text{TEA} + 4\text{H}_2\text{O} \qquad (4)$$

This EC$_{ads}$C$_{mag}$ mechanism indicates that the air oxidation of the Fe(II) intermediate co-deposited with magnetite resulted in the formation of nonstoichiometric magnetite and ferrihydrite found in the previous ex situ study.[9] More generally, the EC$_{ads}$C$_{mag}$ mechanism that is revealed in this study is highly complicated not only by the adsorption of the redox species (eq 3) but also by the surface chemical reaction of the adsorbed species (eq 4). To the best of our knowledge, the adsorption and surface chemical reaction of a redox species were quantitatively investigated only recently by fast-scan cyclic voltammetry (CV) to resolve surface-mediated pathways for the reduction of benzyl chloride at a silver electrode.[20]

Significantly, this in situ, real-time, and quantitative study of electrodeposition and electrodissolution is enabled by employing SECM under transient conditions in contrast to commonly used steady-state conditions, which make the experimental results unperturbed by surface processes.[21] In addition, we employ both substrate generation/tip collection (SG/TC) and feedback modes of SECM (Figure 1) to kinetically resolve electrodeposition and electrodissolution, respectively, under high mass-transport conditions across micrometer-wide tip−substrate gaps. The amperometric current at a Au tip is measured against the cycled potential of a macroscopic Au substrate and analyzed by the finite element method.[22] Both adsorption of Fe(II)−TEA and formation of magnetite from the adsorbed Fe(II) intermediate at the substrate surface are included in the numerical analysis to determine all reaction
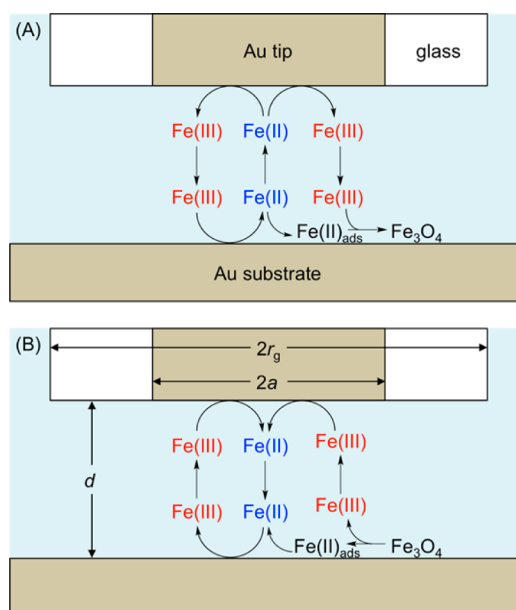

Figure 1. Scheme of SECM tip and substrate for (A) the SG/TC mode based on the electrodeposition of magnetite and (B) the feedback mode based on the electrodissolution of magnetite. Fe(III) and Fe(II) represent Fe(III)−TEA and Fe(II)−TEA, respectively.

parameters of the extremely complicated EC$_{ads}$C$_{mag}$ mechanism from a pair of SECM-based CVs in feedback and SG/TC modes.

■ EXPERIMENTAL SECTION

Chemicals. $\text{FeCl}_3\cdot6\text{H}_2\text{O}$ (>99.0%) from Acros Organics (Fair Lawn, NJ), NaOH from Fisher Scientific (Pittsburgh, PA), and TEA (98%) from Sigma-Aldrich (St. Louis, MO) were used to prepare 5 mM Fe(III)−TEA in 5 M NaOH.[18b] Briefly, the Fe(III)−TEA solution was obtained by dissolving $\text{FeCl}_3\cdot6\text{H}_2\text{O}$ and 2 moles of TEA with respect to moles of the metal ion in ultrapure water bubbled with argon and then by diluting the resultant solution with a NaOH solution. A Milli-Q Integral system (EDM Millipore, Berllerica, MA) was used to obtain ultrapure water with a resistivity of 18.3 MΩ/cm and a total organic carbon level of <3 ppb as measured by internal monitors.

SECM Measurements. A commercial SECM instrument (CHI 920D, CH Instruments, Austin TX) was employed to measure approach curves and SECM-based CVs. An SECM cell was filled with Milli-Q water containing 5 mM Fe(III)−TEA and 5 M NaOH. The solution was purged with Ar for 30 min and was kept under Ar flow during SECM measurements. A 25 μm-diameter Au ultramicroelectrode was fabricated as an SECM tip and characterized by optical microscopy as well as SECM approach curve measurement at an insulating substrate (Figure S-1) to determine tip inner and outer radii, a and r_g, respectively (Figure 1B). The Au tip was polished on soft pads with 3, 1, and 0.5 μm diamond powders, washed with Milli-Q water, ethanol, and Milli-Q water, and kept in Milli-Q water. A 2 mm-diameter Au electrode (CH Instruments) was used as a substrate electrode, which was polished with 0.1 and 0.05 μm aluminum powders on microfiber pads, washed with ethanol and Milli-Q water, and sonicated in Milli-Q water. In addition, a Ag/AgCl quasi reference electrode and a Pt counter electrode were employed. All electrochemical experiments were performed at ~22 °C.

Analysis of SECM-Based CV. Experimental SECM-based CVs were fitted with SECM-based CVs simulated by the finite element method using COMSOL Multiphysics 5.3 (COMSOL, Burlington, MA). A fit was evaluated by visually comparing experimental and simulated SECM-based CVs. In addition, we evaluated the fit by the method of least-squares based on the Optimization module of

COMSOL Multiphysics.[23] Both fitting methods required 100−300 iterations to find the best set of parameters from wide ranges of parameter values.

RESULTS AND DISCUSSION

No Electrodeposition of Magnetite in the Positive Feedback Mode. The positive feedback mode of SECM was used in this study as well as in previous SECM studies[24] to precisely position a tip at a short distance from a substrate in an alkaline Fe(III)−TEA solution without the electrodeposition of magnetite. The $EC_{ads}C_{mag}$ mechanism proposed in this study indicates that the positive feedback mode does not cause the electrodeposition of magnetite at a tip or a substrate, where Fe(III)−TEA or Fe(II)−TEA is depleted, respectively. In this operation mode, we set the tip potential, E_T, at −1.15 V to exhaustively reduce Fe(III)−TEA to Fe(II)−TEA at a diffusion-limited rate as expected from the CV of the tip in the bulk solution (the inset of Figure 2). Subsequently,
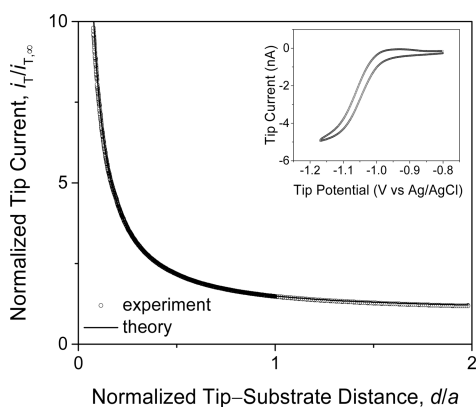

Figure 2. Experimental (circles) and theoretical (solid line) SECM approach curves in the positive feedback mode as obtained with a 25 μm-diameter Au tip (RG = 3.0) over a 2 mm-diameter Au substrate in a 5 M NaOH solution containing 5 mM Fe(III)−TEA. E_T = −1.15 V and E_S = −0.8 V vs Ag/AgCl. Probe scan rate, 50 nm/s. The inset shows a CV at the tip in the Fe(III)−TEA solution at a potential sweep rate of 25 mV/s.

Fe(III)−TEA was depleted to yield no magnetite at the tip (eq 4), although Fe(II)−TEA was adsorbed on the tip (eq 3). Moreover, magnetite was not electrodeposited at the substrate, because the substrate potential, E_S, was set at −0.8 V to exhaustively oxidize tip-generated Fe(II)−TEA at a diffusion-limited rate when the tip was positioned near the substrate. Accordingly, no Fe(II)−TEA was available near the substrate surface, thereby preventing the formation of the Fe(II) intermediate (eq 3) and, subsequently, the deposition of magnetite (eq 4).

Experimentally, we controlled the tip−substrate distance, d, by measuring an approach curve in the positive feedback mode (Figure 2), where the amperometric current at a Au tip with a radius, a, of 12.5 μm was monitored as the tip approached to a 2 mm-diameter Au substrate. The approach curve fit very well with a theoretical curve for the positive feedback mode.[25] A good fit was obtained until the tip current, i_T, was enhanced by a factor of 10 with respect to the tip current in the bulk solution, $i_{T,\infty}$, as given by

$$i_{T,\infty} = 4xnFD_{Fe(III)}c_0a \qquad (5)$$

where $x = 1.07$[25] for $RG = r_g/a = 3.0$ (r_g is the outer diameter of the glass tip; Figure 1B), n (= 1) is the number of electron transferred in the tip reaction (eq 1), and $D_{Fe(III)}$ and c_0 are the diffusion coefficient and concentration of Fe(III)−TEA in the bulk solution. The large enhancement of the tip current corresponds to a tip−substrate distance of 1.0 μm. This distance is extremely short with respect to the tip radius, that is, d/a = 0.08, which ensures the flat surface of the sharp tip with thin glass sheath.

SECM-Based Transient CV of Electrodeposition and Electrodissolution of Magnetite. We employed the SG/TC and feedback modes of SECM to investigate the electrodeposition and electrodissolution of magnetite, respectively, at the macroscopic Au substrate during the reductive cycling of the potential in an alkaline solution of Fe(III)−TEA (Figure 1). Preliminarily, we measured SECM-based CVs at various potential sweep rates, v, from 1 mV/s to 500 mV/s to find that v = 25 mV/s is optimum for the quantitative study of magnetite electrodeposition (see Figures S-2 and S-5). In addition, the corresponding dimensionless sweep rate, σ, of 0.76 (eq S-16) was sufficiently low to attain SECM quasi-steady-state conditions owing to relatively small diffusion coefficients of the Fe(III)−TEA/Fe(II)−TEA couple and a short tip−substrate distance of 4.1 μm determined from an approach curve.[22a] This distance corresponds to d/a = 0.33 and was short enough to kinetically resolve each step of the $EC_{ads}C_{mag}$ mechanism. Six pairs of SECM-CVs in SG/TC and feedback modes were obtained reproducibly to reliably obtain all reaction parameters for the $EC_{ads}C_{mag}$ mechanism. By contrast, a reversible CV was obtained by monitoring the substrate current against the substrate potential to yield no kinetic information as well as no feature of the electrodeposition or electrodissolution of magnetite[18] as expected when both electrochemical and chemical steps are diffusion-controlled.[26]

The electrodissolution of magnetite at the Au substrate was directly observed by SECM-based CV in the feedback mode as a peak-shaped current response during the reverse sweep of the substrate potential (red line in Figure 3A). In this measurement, the cathodic tip current based on the reduction of Fe(III)−TEA was monitored during the cycle of the substrate potential from −0.55 V to −1.26 V and then back to −0.55 V. The resultant CV based on the plot of the tip current versus the substrate potential yielded forward and reverse waves with unique shapes. During the forward potential sweep (blue line in Figure 3A), the tip current stayed at the original positive-feedback value from −0.55 V to −0.95 V and then gradually dropped to zero at more negative substrate potentials, which reductively depleted Fe(III)−TEA at the substrate surface and, subsequently, from the tip−substrate gap, that is, a shielding effect.[27] The sigmoidal shape of the forward wave ensured the quasi-steady-state mass transport of Fe(III)−TEA and Fe(II)−TEA across the tip−substrate gap[22a] as well as no adsorption of Fe(III)−TEA on the substrate.[22b,28] Moreover, the forward wave was shifted positive with respect to the corresponding theoretical CV based only on the ET step[22a] (eq 1; see black circles), where $E^{0'}$ = −1.043 V vs Ag/AgCl was determined by the finite element analysis of SECM-based CVs as discussed later. This positive shift is due to the following chemical steps, which thermodynamically facilitate the ET reaction. In fact, the deposition of magnetite based on the chemical steps was evidenced by a peak-shaped voltammetric response during the
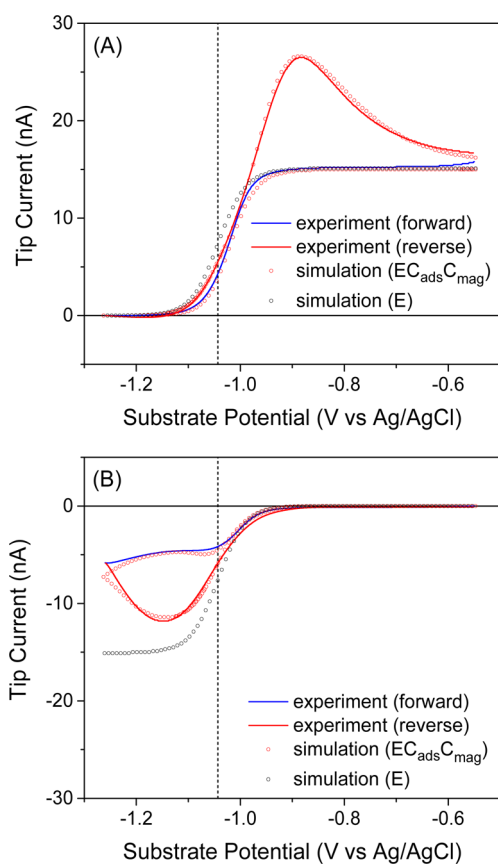
Figure 3. SECM-based CVs in (A) feedback and (B) SG/TC modes with a 25 μm-diameter Au tip over a 2 mm-diameter Au substrate in a 5 M NaOH solution containing 5 mM Fe(III)−TEA. E_T = −1.12 and −0.75 V vs Ag/AgCl for the respective operation modes. Potential sweep rate, 25 mV/s. Switching potential, − 1.26 V vs Ag/AgCl. Black dotted lines represent a formal potential of −1.043 V vs Ag/AgCl. Parameters used for the simulation of CVs based on $EC_{ads}C_{mag}$ and E mechanisms are listed in Table 1.

reverse potential sweep, where Fe(III)−TEA was generated directly by the electrodissolution of magnetite as well as indirectly by the desorption and oxidation of Fe(II)−TEA at the substrate (Figure 1B).

SECM-based CV was performed also in the SG/TC mode to directly observe the electrodeposition of magnetite (Figure 3B). In this operation mode, the amperometric tip current was based on the diffusion-limited oxidation of Fe(II)−TEA, which was depleted to prevent the deposition of magnetite at the tip. A tip current response was obtained when the substrate potential was negative enough to generate Fe(II)−TEA from Fe(III)TEA. The anodic tip current, however, was much lower in the SG/TC mode than in the feedback mode. In fact, the tip current in the SG/TC mode was lower in comparison with the theoretical CV based only on the ET step[22a] (eq 1; see black circles). The tip current in the SG/TC mode was lowered, because Fe(II)−TEA was consumed by its adsorption and conversion to magnetite at the substrate surface (Figure 1A). Interestingly, the tip current was higher during the reverse potential sweep to yield a peak-shaped response (red line). This result indicates that the substrate surface was nearly saturated with the adsorption of Fe(II)−TEA during the forward potential sweep so that less Fe(II)−TEA was adsorbed during the reverse potential sweep, thereby yielding a higher collection efficiency for Fe(II)−TEA at the tip.

Finite Element Analysis Based on the $EC_{ads}C_{mag}$ Mechanism. SECM-based CVs were simulated by employing the finite element method based on COMSOL Multiphysics to reveal that the electrodeposition and electrodissolution of magnetite were based on the $EC_{ads}C_{mag}$ mechanism. In this simulation, an SECM diffusion problem was defined and solved numerically as detailed in Supporting Information. Boundary conditions at the substrate surface were given by using the following rate laws (also see Supporting Information). Heterogeneous reduction and oxidation rate constants, k_{red} and k_{ox}, respectively, were defined for the Fe(III)−TEA/Fe(II)−TEA couple (eq 1) by using the Butler−Volmer model as

$$k_{red} = k_{app}^0 \exp\left[-\frac{\alpha F(E_S - E^{0'})}{RT} \right] \tag{6}$$

$$k_{ox} = k_{app}^0 \exp\left[\frac{(1 - \alpha)F(E_S - E^{0'})}{RT} \right] \tag{7}$$

where k_{app}^0 represents the apparent standard ET rate constant as defined later, α is the transfer coefficient, and $E^{0'}$ is the formal potential. The corresponding ET rate was defined by eq S-2. In addition, we employed the Frumkin isotherm to phenomenologically express rate constants for the adsorption and desorption of Fe(II)−TEA (eq 3), k_{ads} and k_{des}, respectively, as[29]

$$k_{ads} = k \exp\left[\beta g' \frac{\Gamma_{Fe(II)}}{\Gamma_{Fe(II)}^0} \right] \tag{8}$$

$$k_{des} = \frac{k}{\beta_{Fe(II)}} \exp\left[-(1 - \beta)g' \frac{\Gamma_{Fe(II)}}{\Gamma_{Fe(II)}^0} \right] \tag{9}$$

where $\Gamma_{Fe(II)}$ is the surface concentration of the adsorbed Fe(II) intermediate, $\Gamma_{Fe(II)}^0$ is its saturated surface concentration, k is the adsorption rate constant at $\Gamma_{Fe(II)} = 0$, β is the symmetry factor, g' is a parameter that describes interactions between adsorbed Fe(II) intermediates,[30] and $\beta_{Fe(II)}$ is an equilibrium parameter in the isotherm. The corresponding adsorption rate was given by eq S-3. Finally, the rate of magnetite deposition (eq 4) was defined by the forward rate constant, $k_{m,f}$, and an equilibrium constant, K_m (eq S-4).

The finite element analysis based on the $EC_{ads}C_{mag}$ mechanism indicated that ET and chemical steps were kinetically resolvable under high mass-transport conditions of SECM across the tip−substrate gap. SECM-based CVs in both feedback and SG/TC modes fit well with CVs simulated with the $EC_{ads}C_{mag}$ mechanism (Figure 3) to yield a set of eight reaction parameters including rate constants for all steps (Table 1) when the fit was evaluated visually. These parameter values were used as initial values to achieve a slightly better fit (Figure S-4A,B) using similar parameter values (Table S-1) by the method of least-squares based on the Optimization module[23] of COMSOL Multiphysics. This result ensures that a residual sum of squares can be minimized by a unique set of parameter values. In fact, we employed the method of least-squares to demonstrate that only narrow ranges of the reaction parameters (typically 10%−20% with respect to the best values; see Table S-1) give good fits for both feedback and SG/TC branches of SECM-based CVs. This assessment showed that $k_{m,f}$ was the

Table 1. Reaction Parameters of Magnetite Electrodeposition Determined from Both Feedback and SG/TC Branches of SECM-Based CV[a]

k^0 (cm/s)	0.13	g'	3.3
$E^{0'}$ (V vs Ag/AgCl)	−1.043	$\Gamma_{Fe(II)}^0$ (10^{-9} mol/cm^2)	5.4
k (10^5 cm^3/s/mol)	2.2	$k_{m,f}$ (10^{10} cm^6/s/mol^2)	1.1
$\beta_{Fe(II)}$ (10^5 cm^3/mol)	1.5	K_m (10^{10} cm^6/mol^2)	2.1

[a]All parameters were used for the simulation of the $EC_{ads}C_{mag}$ mechanism in Figure 3, where only k^0 and $E^{0'}$ were used for the E mechanism.

most variable parameter among the eight parameters, but was varied only by <35% with respect to the best value to fit both branches. Moreover, other parameters were separately determined or approximated for simplicity to augment the reliability of the finite element analysis. Specifically, the limiting current of the forward wave of the feedback mode (Figure 3A) was used to yield a gap width, d, of 4.1 μm using a known $D_{Fe(III)}$ value of 2.0×10^{-6} cm^2/s[24b] as well as tip radii of a = 12.5 μm and r_g = 3.0a determined from approach curves at insulating substrates (Figure S-1). A $D_{Fe(II)}$ value of 2.0×10^{-6} cm^2/s (= $D_{Fe(III)}$), a theoretical α value of 0.5,[31] and a presumed β value of 0.5[29] were employed for simplicity.

We obtained additional evidence to support the $EC_{ads}C_{mag}$ mechanism against EC mechanisms. Specifically, we employed different potential sweep rates between 5 mV/s and 50 mV/s at a shorter tip−substrate distance of 2.1 μm to demonstrate that the resultant SECM-based CVs fit well with theoretical CVs based on the $EC_{ads}C_{mag}$ mechanism (Figure S-5). Reaction parameters thus obtained (Table S-2) were similar among different potential sweep rates and were also similar to those obtained at a longer tip−substrate distance of 4.1 μm (Table 1). Moreover, $\Gamma_{Fe(II)}^0$ values determined by SECM-based CV were consistent with a value determined by double potential step chronocoulometry (Figure S-6). By contrast, a good fit was not obtainable by assuming the EC mechanisms where the chemical step included only adsorption of Fe(II)−TEA (eq 3) without the formation of magnetite (Figure S-7) or one-step deposition of magnetite (eq 2) as considered previously[9,14] (Figure S-8).

The finite element analysis of the SG/TC branch demonstrated that the ET step (eq 1) was reversible during the forward potential sweep and then became kinetically controlled during the reverse potential sweep when the substrate surface was significantly covered with the adsorbed Fe(II) intermediate. This result indicates an inhibitory effect from the adsorbed Fe(II) intermediates, which was assumed in the finite element analysis to prevent the ET step, thereby yielding[32]

$$k_{app}^0 = k^0 \left[1 - \frac{\Gamma_{Fe(II)}}{\Gamma_{Fe(II)}^0} \right] \tag{10}$$

where k^0 is the true standard ET rate constant. No consideration of the inhibitory effect significantly compromised a fit of the reverse wave of the SG/TC mode with simulation (see Figure S-9 with $k_{app}^0 = k^0$). A chemical origin of this inhibitory effect is that the adsorbed Fe(II) intermediate is a nonconductive oxide or hydroxide[33] in contrast to conductive magnetite.[10] In fact, the co-deposit of Fe(II)-based hydroxides with magnetite is compositionally consistent with electrodeposited green rust, for example, $Fe_6(OH)_{12}SO_4 \cdot nH_2O$, which contains an excess amount of Fe(II) with respect to Fe(III) in

comparison with magnetite to produce ferrihydrite through air oxidation as proposed in the previous ex situ study.[9] Moreover, the slow adsorption and desorption of Fe(II)−TEA are attributed to the presence of the adsorbed Fe(II) intermediate as an oxide or a hydroxide. This adsorption mechanism is supported by strong attractive interactions as indicated by a g' value of 3.3, which is more positive than general values of $-2 \leq g' \leq 2$.[30a] A negative g' value is expected for the adsorption of Fe(II)−TEA or Fe(II) ion owing to electrostatic repulsions between the divalent cations.

Potential-Dependent Electrodeposition and Electro-dissolution of Magnetite. Interestingly, the finite element analysis of SECM-based CVs revealed that magnetite was electrodeposited and then completely electrodissolved during both forward and reverse sweeps of the substrate potential. To make this finding, we calculated the normalized flux based on the deposition and dissolution of magnetite, J_m, at the substrate surface under the tip (see Supporting Information) by using the parameters determined from SECM-based CVs (Table 1). In addition, we calculated the normalized flux based on the adsorption and desorption of Fe(II)−TEA, J_{ads}, which were coupled with the deposition and dissolution of magnetite, respectively. These fluxes were calculated by integrating the corresponding fluxes over the substrate surface under the Au tip including the glass sheath, because electrochemical and chemical steps at this local region of the substrate surface contributed to the tip current (see below). The fluxes were plotted against the substrate potential (Figure 4A,B) such that a negative flux corresponded to the deposition of magnetite or the adsorption of Fe(II)−TEA, whereas a reverse process yielded a positive flux. Identical plots were obtained for feedback and SG/TC modes.

We found that a relatively small amount of magnetite was formed and completely dissolved during the forward potential sweep (Figure 4A), while Fe(II)−TEA was continuously adsorbed at the substrate surface (Figure 4B). As the substrate potential was swept toward the formal potential of the Fe(III)−TEA/Fe(II)−TEA couple (black dotted lines), the reduction of Fe(III)−TEA to Fe(II)−TEA was initiated at the substrate surface to adsorb Fe(II)−TEA. The adsorbed species served as a precursor to deposit magnetite with Fe(III)−TEA, which was still abundant near the substrate surface. Magnetite, however, started to dissociate as the substrate potential was swept beyond the formal potential because of the depletion of Fe(III)−TEA near the substrate surface. Eventually, magnetite was completely dissolved at −1.2 V to yield the zero flux. Significantly, this result is consistent with a previous report that no magnetite was deposited at the cathode of an alkaline redox flow battery during the charging process based on the exhaustive reduction of Fe(III)−TEA at < −1.2 V.[18b]

In comparison to the forward sweep, a much larger amount of magnetite was electrodeposited during the reverse sweep (Figure 4A), because the substrate surface was already covered with a large amount of the adsorbed Fe(II) intermediate at the switching potential (Figure 4B). As the substrate potential was swept from the switching potential to the formal potential, Fe(III)−TEA was generated at the substrate surface to initiate the formation of magnetite with the adsorbed Fe(II) intermediate, which was partially desorbed owing to the consumption of Fe(II)−TEA. Magnetite continued to grow until the substrate potential reached to −0.95 V. As the substrate potential became more positive, Fe(II)−TEA was depleted significantly to drive not only its desorption but also
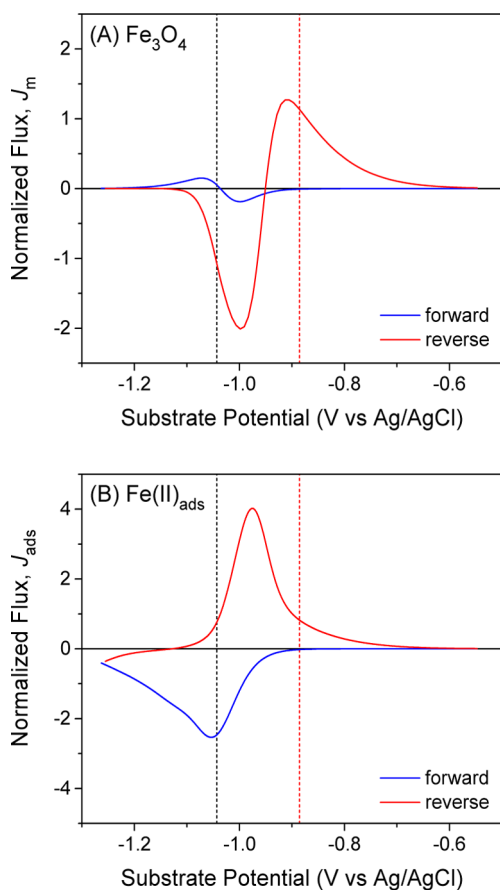
Figure 4. Normalized fluxes simulated for (A) the deposition and dissolution of magnetite and (B) the adsorption and desorption of Fe(II)−TEA at the substrate under the whole tip including Au and glass sheath. The parameters used for this simulation are listed in Table 1. Black dotted lines represent a formal potential of −1.043 V vs Ag/AgCl, whereas red dotted lines indicate a peak potential of −0.882 V vs Ag/AgCl in the feedback mode of SECM-based CV during the reverse potential sweep (see Figure 3A).

the dissolution of magnetite. Eventually, the substrate surface became free from both magnetite and the adsorbed Fe(II) intermediate at −0.6 V to yield the zero flux for both species. This result accounts for no electrodeposition of magnetite at the anode of an alkaline redox flow battery during the discharging process based on the diffusion-limited oxidation of Fe(II)−TEA at −0.4 V.[18b]

The finite element analysis showed that a voltammetric peak at −0.88 V during the reverse potential sweep in the feedback mode (Figure 3A) was due to the dissolution of magnetite and was not simply due to the desorption of Fe(II)−TEA. In fact, the flux based on the desorption of Fe(II)−TEA peaked at −0.98 V (Figure 4B), which was more positive than the formal potential to immediately oxidize Fe(II)−TEA to Fe(III)−TEA. The corresponding tip current, however, increased only moderately (Figure 3A), because Fe(III)−TEA was consumed by the formation of magnetite at this potential (Figure 4A). By contrast, a peak potential of −0.88 V was positive enough not only to desorb Fe(II)−TEA but also to dissolve magnetite (Figure 4A), thereby producing Fe(III)−TEA directly from magnetite as well as indirectly by the oxidation of Fe(II)−TEA dissociated from magnetite. In fact, the finite element simulation showed that the dissolution of magnetite at the peak potential raised the concentration of Fe(III)−TEA near

the substrate surface beyond its bulk concentration (Figure 5A), whereas the corresponding concentration of Fe(II)−TEA
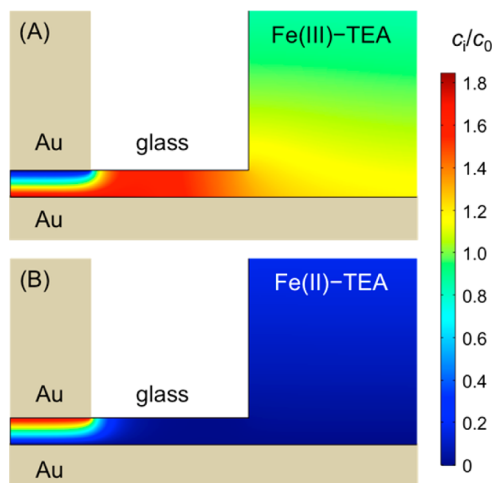

Figure 5. Concentration profiles of (A) Fe(III)−TEA and (B) Fe(II)−TEA in the tip−substrate gap at a peak potential of −0.882 V vs Ag/AgCl during the reverse potential sweep in the feedback mode (see Figure 3A). The scale bar indicates the concentration of Fe(III)−TEA and Fe(II)−TEA, c_i, with respect to the concentration of Fe(III)−TEA in the bulk solution, c_0.

was nearly zero (Figure 5B). This simulation also demonstrated that a high concentration of Fe(III)−TEA was accumulated under the glass sheath surrounding the Au tip (Figure 5A) to eventually contribute to the peak-shaped current response. Accordingly, a higher peak-shaped current response was obtained when a thicker glass sheath, that is, larger RG, was employed in the simulation.

Surface Chemical Reactions of Adsorbed Redox Species. The $EC_{ads}C_{mag}$ mechanism revealed by SECM-based CV in this study is highly complicated not only by the adsorption of a redox species on the substrate surface (eq 3) but also by the chemical reaction of the adsorbed species at the surface (eq 4). In fact, this work is the first to investigate a surface chemical reaction of adsorbed species by SECM-based CV, which was developed recently to investigate simple ET reactions at macroscopic substrates under quasi-steady-state conditions[22a] as well as preceding[22b,28] and following[34] adsorption steps under transient conditions without a coupled chemical reaction of adsorbed species at the substrate surface. In this study, SECM-based CVs with unusual shapes (e.g., Figure 3) were simulated by considering the $EC_{ads}C_{mag}$ mechanism to reveal the importance of a surface chemical reaction of adsorbed redox species in the electrodeposition of functional compound materials. To the best of our knowledge, the adsorption and coupled chemical reaction of a redox species at the electrode surface were quantitatively investigated only recently in the fast-scan CV study of the surface-mediated reduction of benzyl chloride at a silver electrode.[20] Note that the ECC mechanism is typically based only on homogeneous chemical reactions[35] and rarely involves an adsorption step[36] to analyze experimental results.

It should be noted that a surface chemical reaction of an adsorbed redox species can be represented by a heterogeneous ET reaction of an adsorbed species with a solution species as given by
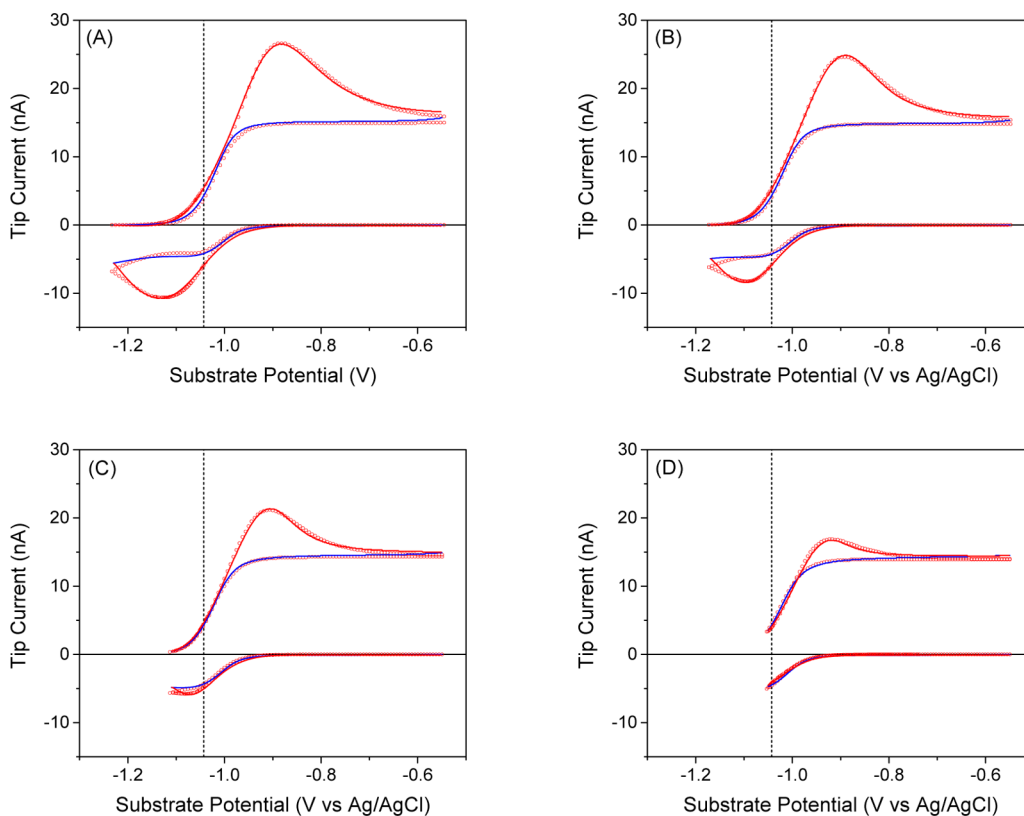
Figure 6. SECM-based CVs in feedback and SG/TC modes at various switching potentials as obtained with a 25 μm-diameter Au tip over a 2 mm-diameter Au substrate in a 5 M NaOH solution containing 5 mM Fe(III)−TEA. E_T = −1.12 and −0.75 V vs Ag/AgCl for the respective operation modes. Switching potentials are (A) −1.23, (B) −1.17, (C) −1.11, and (D) −1.05 V vs Ag/AgCl. Potential sweep rate, 25 mV/s. Blue and red lines represent the forward and reverse branches of experimental CVs, respectively, whereas simulated CVs are shown by circles.

$$R_{ads} + O' \rightleftharpoons O_{ads} + R' \qquad\qquad (11)$$

where the underlying electrode is not involved directly. This type of surface reactions has been quantitatively treated for the surface-interrogation (SI) mode of SECM to determine the surface coverage of adsorbed redox species.[24,33,37] These reactions, however, are simplified mechanistically in SI-SECM, where the spontaneous desorption of the adsorbed species is prevented experimentally to neglect the adsorption/desorption step in data analysis. By contrast, the reversible adsorption of a redox species was coupled with a heterogeneous self-exchange reaction (HSER; $R_{ads} + O \rightleftharpoons O_{ads} + R$) in recent CV[38] and SECM-based CV[28] studies. These studies, however, were not able to experimentally verify HSERs, which were thermodynamically forbidden or electrochemically uninfluential.[39] In this study, we did not consider a HSER of the Fe(III)−TEA/Fe(II)−TEA couple at the substrate, where only Fe(II)−TEA was adsorbed to thermodynamically prevent the HSER.[22b,39a]

Effect of Switching Potential. We studied the electrodeposition and electrodissolution of magnetite at various switching potentials to examine how reaction parameters depend on the progression of electrodeposition, which changes the substrate surface from bare gold to a co-deposit of magnetite with the adsorbed Fe(II) intermediate. We systematically changed the switching potential from −1.02 V to −1.26 V every 0.03 V to obtain nine pairs of SECM-based CVs in feedback and SG/TC modes (see Figures 3, 6, and S-10). Six pairs of CVs were measured with each switching potential to ensure good reproducibility. Qualitatively, a more negative

switching potential enhanced the adsorption of Fe(II)−TEA during the forward potential sweep so that a larger amount of magnetite was electrodeposited during the reverse potential sweep, which yielded a higher voltammetric peak based on the dissolution of magnetite in the feedback mode. Importantly, the feedback branch of SECM-based CV indicates that the final potential of −0.55 V ensures the complete dissolution of magnetite as well as the complete desorption of Fe(II)−TEA (Figure 4), thereby reproducing a clean substrate surface for the next CV run. Accordingly, the final potential of the SG/TC branch must be also positive enough even though no current response is seen at > −0.90 V.

All experimental CVs fitted well with CVs simulated for the EC$_{ads}$C$_{mag}$ mechanism to find that $\Gamma^0_{Fe(II)}$, g', $\beta_{Fe(II)}$, and K_m depended on the switching potential (Table S-4). Specifically, a $\Gamma^0_{Fe(II)}$ value of 2.8 × 10^{-9} mol/cm^2 at the most positive switching potential of −1.02 V was very similar to the surface concentration of Au atoms at the substrate, for example, 2.5 × 10^{-9} mol/cm^2 of a Au(111) surface. As the switching potential was changed from −1.02 V to −1.26 V, magnetite was not only deposited but also completely dissolved during the forward potential sweep (Figure 4A). By contrast, the formation of the adsorbed Fe(II) intermediate continued even at −1.26 V (Figure 4B) to increase $\Gamma^0_{Fe(II)}$ to 5.3 × 10^{-9} mol/cm^2, which is attributed to nucleation of the adsorbed Fe(II) intermediate, thereby preluding the formation of magnetite. Accordingly, a slightly lower $\beta_{Fe(II)}$ value with a more negative switching potential indicates a weaker attractive interaction of Fe(II)−TEA with the gold surface with more nuclei. The adsorption step, however, is also facilitated by a stronger attractive

interaction between adsorbed Fe(II) intermediates with a more negative switching potential as indicated by a more positive g' value. Finally, K_m increases with a more negative switching potential to reflect the facilitated formation of magnetite on the nuclei.

In Situ and ex Situ Studies of Magnetite Electrodeposition. The $EC_{ads}C_{mag}$ mechanism of magnetite electrodeposition was revealed in this in situ electrochemical study and is also supported by the previous ex situ spectroscopic study of electrodeposited magnetite.[9] In this study, we employed SECM-based CV to detect the adsorbed Fe(II) intermediate, which was not reported in the previous ex situ study of electrodeposited magnetite by X-ray diffraction, scanning electron microscopy, and Mössbauer spectroscopy.[9] The previous study, however, demonstrated that electrodeposited magnetite contained an excess amount of Fe(III), which we attribute to the air oxidation of the adsorbed Fe(II) intermediate. Similarly, the observation of ferrihydrite, for example, $Fe_{10}O_{14}(OH)_2$, in the previous ex situ study can be attributed to the air oxidation of the Fe(II) intermediate co-deposited with magnetite. In fact, the composition of the co-deposited material is consistent with that of green rust,[9] which contains a higher ratio of Fe(II) with respect to Fe(III) than magnetite. It should be noted that the adsorbed Fe(II) intermediate can be oxidized not only ex situ but also in situ by residual oxygen in the alkaline Fe(III)−TEA solution (eq 11) when the underlying substrate is still biased at highly negative potentials or unbiased after the completion of electrodeposition. In this study, we carefully removed oxygen from the solution by not only purging the solution with Ar but also leaving the Ar flow over the solution during the entire SECM experiment.

CONCLUSIONS

Here, we demonstrated the application of SECM to the in situ, real-time, and quantitative study of electrodeposition and electrodissolution that were voltammetrically driven across a wide range of substrate potential. The potential dependence of electrodeposition or electrodissolution was not assessed in previously SECM studies of electrochemical dissolution of metal substrates under unbiased conditions[40] and chemical dissolution of ionic crystals without electron transfer.[41] Significantly, we revealed that the electrodeposition of a multifunctional compound material, that is, magnetite, from an alkaline Fe(III)−TEA solution requires the preceding formation of the Fe(II) intermediate adsorbed on the substrate surface and, subsequently, is mediated through the $EC_{ads}C_{mag}$ mechanism rather than the EC mechanism.[9,14] The high mass-transport condition and high data quality of SECM-based CV were crucial to quantitatively determine reaction parameters for all steps of the $EC_{ads}C_{mag}$ mechanism through the finite element analysis. By contrast, the adsorbed Fe(II) intermediate was not resolvable from co-deposited magnetite by CV only or double potential step chronocoulometry. Moreover, no observation of the adsorbed Fe(II) intermediate in the previous ex situ study of electrodeposited magnetite[9] indicates that this intermediate was oxidized by oxygen in air or solution to yield nonstoichiometric magnetite or ferrihydrite.

Generally, SECM is a powerful technique to diagnose reaction mechanisms, because two electrodes, for example, a generator and a collector, are used instead of a single one, providing more useful information. The steady-state mode of SECM has been used to study the solution intermediates generated at the tip or the substrate.[42] For these applications, steady-state conditions are useful, because the electrochemical results are not perturbed by surface processes such as adsorption and desorption.[21a] However, as shown here, by adding transient measurements, that is, time as a variable, one can deal with very complex systems, for example, involving the electrodeposition and electrodissolution of a compound material, and even detect adsorbed surface intermediates as well. Subsequently, the highly complicated $EC_{ads}C_{mag}$ mechanism based on the surface chemical reaction of adsorbed redox species was revealed by SECM-based CV in this study. The powerful combination of SECM with CV under transient conditions will be useful for the in situ characterization of various electrodeposited compounds to complement their ex situ characterization.

ASSOCIATED CONTENT

Ⓢ Supporting Information

The Supporting Information is available free of charge on the ACS Publications website at DOI: 10.1021/jacs.7b08835.

SECM characterization of tip radii, model and dimensionless parameters used for the finite element simulation of the $EC_{ads}C_{mag}$ mechanism, finite element analysis of SECM-based CVs by the method of least-squares, SECM-based CVs with different potential sweep rates and a different tip−substrate distance, double potential step chronocoulometry of the adsorbed Fe(II) intermediate, finite element analysis based on EC mechanisms, finite element simulation of SECM-based CVs without inhibitory effect of the adsorbed Fe(II) intermediate on ET kinetics, and definitions of fluxes simulated for chemical steps at the substrate surface and SECM-based CVs with different switching potentials (PDF)

AUTHOR INFORMATION

Corresponding Author

*E-mail: ajbard@cm.utexas.edu.

ORCID Ⓘ

Shigeru Amemiya: 0000-0001-7357-4505

Allen J. Bard: 0000-0002-8517-0230

Notes

The authors declare no competing financial interest.

REFERENCES

(1) Switzer, J. A. Electrodeposition at the Nanoscale. In *Nanoelectrochemistry*; Mirkin, M. V.; Amemiya, S., Eds.; CRC Press: Boca Raton, FL, 2015; p 601.

(2) (a) Burke, M. S.; Enman, L. J.; Batchellor, A. S.; Zou, S.; Boettcher, S. W. *Chem. Mater.* **2015**, *27*, 7549. (b) Roger, I.; Shipman, M. A.; Symes, M. D. *Nat. Rev. Chem.* **2017**, *1*, 0003.

(3) Rajeshwar, K.; de Tacconi, N. R.; Chenthamarakshan, C. R. *Chem. Mater.* **2001**, *13*, 2765.

(4) Koza, J. A.; Hill, J. C.; Demster, A. C.; Switzer, J. A. *Chem. Mater.* **2016**, *28*, 399.

(5) Morales-Guio, C. G.; Hu, X. *Acc. Chem. Res.* **2014**, *47*, 2671.

(6) Roger, I.; Symes, M. D. *J. Mater. Chem. A* **2016**, *4*, 6724.

(7) Pandey, R. K.; Sahu, S. N.; Chandra, S. *Handbook of Semiconductor Electrodeposition*; Marcel Dekker: New York, 1996.

(8) Paunovic, M.; Schlesinger, M. *Fundamentals of Electrochemical Deposition*; John Wiley & Sons: New York, 1998.

(9) Kulp, E. A.; Kothari, H. M.; Limmer, S. J.; Yang, J.; Gudavarthy, R. V.; Bohannan, E. W.; Switzer, J. A. *Chem. Mater.* **2009**, *21*, 5022.

(10) Cornell, R. M.; Schwertmann, U. *The Iron Oxides*; VCH: Weinheim, Germany, 1996.

(11) (a) Sorenson, T. A.; Morton, S. A.; Waddill, G. D.; Switzer, J. A. *J. Am. Chem. Soc.* **2002**, *124*, 7604. (b) Switzer, J. A.; Gudavarthy, R. V.; Kulp, E. A.; Mu, G.; He, Z.; Wessel, A. J. *J. Am. Chem. Soc.* **2010**, *132*, 1258. (c) Gudavarthy, R. V.; Miller, A. S.; Bohannan, E. W.; Kulp, E. A.; He, Z.; Switzer, J. A. *Electrochim. Acta* **2011**, *56*, 10550.

(12) (a) Vago, E. R.; Calvo, E. J. *J. Electroanal. Chem.* **1992**, *339*, 41. (b) Wu, Z.-S.; Yang, S.; Sun, Y.; Parvez, K.; Feng, X.; Müllen, K. *J. Am. Chem. Soc.* **2012**, *134*, 9082. (c) Zhang, X.; Wang, X.; Le, L.; Ma, A.; Lin, S. *J. Mater. Chem. A* **2015**, *3*, 19273.

(13) Zhao, C.; Ma, Y.; Shen, C.; Han, W. *J. Nanosci. Nanotechnol.* **2016**, *16*, 950.

(14) Kothari, H. M.; Kulp, E. A.; Limmer, S. J.; Poizot, P.; Bohannan, E. W.; Switzer, J. A. *J. Mater. Res.* **2006**, *21*, 293.

(15) Duan, H. A.; Chen, X. P.; Li, B. Q.; Liang, J. Y. *Mater. Res. Bull.* **2010**, *45*, 1696.

(16) Gudavarthy, R. V.; Gorantla, S.; Mu, G.; Kulp, E. A.; Gemming, T.; Eckert, J.; Switzer, J. A. *Chem. Mater.* **2011**, *23*, 2017.

(17) Jeon, S. H.; Song, G. D.; Hur, D. H. *Mater. Trans.* **2015**, *56*, 1107.

(18) (a) Wen, Y. H.; Zhang, H. M.; Qian, P.; Zhou, H. T.; Zhao, P.; Yi, B. L.; Yang, Y. S. *Electrochim. Acta* **2006**, *51*, 3769. (b) Arroyo-Currás, N.; Hall, J. W.; Dick, J. E.; Jones, R. A.; Bard, A. J. *J. Electrochem. Soc.* **2015**, *162*, A378. (c) Gong, K.; Xu, F.; Grunewald, J. B.; Ma, X.; Zhao, Y.; Gu, S.; Yan, Y. *ACS Energy Lett.* **2016**, *1*, 89.

(19) (a) Bard, A. J.; Mirkin, M. V. *Scanning Electrochemical Microscopy*, 2nd ed.; Taylor and Francis: New York, 2012. (b) Zoski, C. G. *J. Electrochem. Soc.* **2016**, *163*, H3088.

(20) (a) Huang, Y.-F.; Wu, D.-Y.; Wang, A.; Ren, B.; Rondinini, S.; Tian, Z.-Q.; Amatore, C. *J. Am. Chem. Soc.* **2010**, *132*, 17199. (b) Klymenko, O. V.; Buriez, O.; Labbe, E.; Zhan, D. P.; Rondinini, S.; Tian, Z. Q.; Svir, I.; Amatore, C. *ChemElectroChem* **2014**, *1*, 227.

(21) (a) Bard, A. J. Introduction and Principles. In *Scanning Electrochemical Microscopy*, 2nd ed.; Bard, A. J.; Mirkin, M. V., Eds. Taylor and Francis: New York, 2012; p 1. (b) Unwin, P. R.; Bard, A. J. *J. Phys. Chem.* **1992**, *96*, 5035.

(22) (a) Nioradze, N.; Kim, J.; Amemiya, S. *Anal. Chem.* **2011**, *83*, 828. (b) Chen, R.; Balla, R. J.; Li, Z.; Liu, H.; Amemiya, S. *Anal. Chem.* **2016**, *88*, 8323.

(23) (a) *COMSOL 5.3 Optimization Module User's Guide*; COMSOL, Inc.: Burlington, MA2017. (b) McDonald, T. D.; Bayer, C.; DeLee, A. M.; Atchison, E.; Widrig, D.; Hutchens, B.; Leonard, K. C. *J. Electrochem. Soc.* **2016**, *163*, H359.

(24) (a) Ahn, H. S.; Bard, A. J. *J. Am. Chem. Soc.* **2016**, *138*, 313. (b) Arroyo-Currás, N.; Bard, A. J. *J. Phys. Chem. C* **2015**, *119*, 8147.

(25) Lefrou, C. A. *J. Electroanal. Chem.* **2006**, *592*, 103.

(26) Bard, A. J.; Faulkner, L. R. *Electrochemical Methods: Fundamentals and Applications*, 2nd ed.; John Wiley & Sons: New York, 2001; p 496.

(27) Zoski, C. G.; Aguilar, J. C.; Bard, A. J. *Anal. Chem.* **2003**, *75*, 2959.

(28) Tan, S.-Y.; Zhang, J.; Bond, A. M.; Macpherson, J. V.; Unwin, P. R. *Anal. Chem.* **2016**, *88*, 3272.

(29) Gileadi, E. *Electrode Kinetics for Chemists, Chemical Engineers and Materials Scientists*; VCH: New York, 1993; p 271.

(30) (a) Bard, A. J.; Faulkner, L. R. *Electrochemical Methods: Fundamentals and Applications*, 2nd ed.; John Wiley & Sons: New York, 2001; p 567. (b) Retter, U. *J. Electroanal. Chem. Interfacial Electrochem.* **1987**, *236*, 21. (c) Yang, C. *J. Phys. Chem.* **1993**, *97*, 7097.

(31) Bard, A. J.; Faulkner, L. R. *Electrochemical Methods: Fundamentals and Applications*, 2nd ed.; John Wiley & Sons: New York, 2001; p 121.

(32) Amatore, C.; Savéant, J. M.; Tessier, D. *J. Electroanal. Chem. Interfacial Electrochem.* **1983**, *147*, 39.

(33) Rodriguez-Lopez, J.; Minguzzi, A.; Bard, A. J. *J. Phys. Chem. C* **2010**, *114*, 18645.

(34) Brites Helú, M. A.; Bonazza, H. L.; Fernández, J. L. *J. Electroanal. Chem.* **2016**, *775*, 64.

(35) Bieniasz, L. K. *Modelling Electroanalytical Experiments by the Integral Equation Method*; Springer: New York, 2015.

(36) (a) Bhugun, I.; Lexa, D.; Savéant, J.-M. *J. Am. Chem. Soc.* **1996**, *118*, 1769. (b) Bhugun, I.; Savéant, J.-M. *J. Electroanal. Chem.* **1996**, *408*, 5.

(37) (a) Rodriguez-Lopez, J.; Alpuche-Aviles, M. A.; Bard, A. J. *J. Am. Chem. Soc.* **2008**, *130*, 16985. (b) Rodriguez-Lopez, J. Surface Interrogation Mode of Scanning Electrochemical Microscopy (SI-SECM): An Approach to the Study of Adsorption and (Electro)-Catalysis at Electrodes. In *Electroanalytical Chemistry: A Series of Advances*; Bard, A. J., Zoski, C., Eds.; CRC Press-Taylor & Francis Group: Boca Raton, 2012; Vol. 24, p 287. (c) Nunige, S.; Cornut, R.; Hazimeh, H.; Hauquier, F.; Lefrou, C.; Combellas, C.; Kanoufi, F. *Angew. Chem., Int. Ed.* **2012**, *51*, 5208.

(38) Cuharuc, A. S.; Zhang, G.; Unwin, P. R. *Phys. Chem. Chem. Phys.* **2016**, *18*, 4966.

(39) (a) Amemiya, S. *Anal. Chem.* **2017**, *89*, 7269. (b) Laviron, E.; Roullier, L. *J. Electroanal. Chem.* **1998**, *443*, 195.

(40) Cornut, R.; Nunige, S.; Lefrou, C.; Kanoufi, F. *Electrochim. Acta* **2011**, *56*, 10701.

(41) McGeouch, C. A.; Edwards, M. A.; Mbogoro, M. M.; Parkinson, C.; Unwin, P. R. *Anal. Chem.* **2010**, *82*, 9322.

(42) Cao, F. H.; Kim, J.; Bard, A. J. *J. Am. Chem. Soc.* **2014**, *136*, 18163.